

The hyperbolic Voronoi diagram in arbitrary dimension*

Frank Nielsen[†]

Richard Nock[‡]

Abstract

We show that in the Klein ball model of hyperbolic space, the hyperbolic Voronoi diagram is affine and amounts to clip a corresponding power diagram, requiring however algebraic arithmetic. By considering the lesser-known Beltrami hemisphere model of hyperbolic geometry, we overcome the arithmetic limitations of Klein construction. Finally, we characterize the bisectors and (pre)geodesics in the other Poincaré upper half-space, the Poincaré ball, and the Lorentz hyperboloid models, and discusses degenerate cases for which the dual hyperbolic Delaunay complex is not a triangulation.

Keywords: Hyperbolic geometry; Voronoi diagram; power diagram; affine diagram; Möbius diagram; Delaunay complex; Delaunay triangulation; hemisphere model; Klein ball model; Poincaré ball model; upper halfspace model; Lorentz hyperboloid model; geodesic metric space.

1 Introduction

Given a finite distinct point set $\mathcal{P} = \{p_1, \dots, p_n\}$ of a space \mathbb{X} equipped with a distance function $d(\cdot, \cdot)$, the Voronoi diagram [12] of \mathcal{P} tessellates¹ the space into proximity regions called Voronoi cells. The Voronoi cell of point p is defined by

$$\text{Vor}(p) := \{x \in \mathbb{X} \mid d(p, x) \leq d(q, x), \forall q \in \mathcal{P}\}, \forall p \in \mathcal{P}. \quad (1)$$

The ordinary d -dimensional Voronoi diagram is obtained by taking the Euclidean distance $d(p, q) = \|p - q\|_E := \sqrt{\langle p - q, p - q \rangle_E} = \sqrt{\sum_{i=1}^d (p_i - q_i)^2}$ (square root of the Euclidean inner product of the vector difference). This Euclidean Voronoi diagram has been extensively studied [26] in relation with the Delaunay triangulation. The Delaunay triangulation [16] $\text{DT}(\mathcal{P})$ of a point set \mathcal{P} is defined as a triangulation such that no point of \mathcal{P} falls strictly inside the circumscribing spheres of its simplices anchored at \mathcal{P} . The Delaunay triangulation is unique for points in general position² (no collinear nor co-spherical degeneracies).

*In this revised manuscript, we added the geodesic equation for the Klein geodesics and the connection of hyperbolic geometry with the special spaces of symmetric positive-definite matrices with prescribed determinants.

[†]Corresponding author. Fax:(+81) 3-5448-4380. Frank.Nielsen@acm.org. Sony Computer Science Laboratories Inc., 3-14-13 Higashi Gotanda 3F, Shinagawa-Ku, Tokyo 141-0022, Japan.

[‡]Richard.Nock@martinique.univ-ag.fr. CEREGMIA UAG, Campus de Schoelcher, BP 7209. 97275 Schoelcher, Martinique, France.

¹Pairwise disjoint interior tiles fully covering \mathbb{X} .

²That is, no k -flat containing $k+2$ points of \mathcal{P} and no k -sphere passing through $k+3$ points of \mathcal{P} (for $1 \leq k \leq d-1$).

In this work, we consider the Voronoi diagram in the d -dimensional real hyperbolic geometry space $\mathbb{X} = \mathbb{H}^d(\kappa)$ of constant negative sectional curvature³ κ . We refer the reader to the survey [14] for a concise description of the five standard models of hyperbolic geometry with their relationships. We call those five models as follows:

- the Poincaré Upper half-space (U),
- the Poincaré Ball (P),
- the Klein ball (K),
- the Lorentz hyperboloid (L), and
- the Beltrami hemisphere models (B).

The above B/K/L/P/U naming and mnemonic of those models does not necessarily reflect the historical development of non-euclidean geometry. See [24] for a historical perspective of the first 150 years of hyperbolic geometry.

The paper is organized as follows: Section 1.1 briefly recalls prior work concerning the hyperbolic Voronoi diagram in arbitrary dimension, and section 1.2 motivates the study of hyperbolic Voronoi diagrams by presenting some applications ranging from computer graphics to computational information geometry and machine learning. Section 2 describes the hyperbolic Voronoi diagram in the hemisphere model and show how to compute it using off-the-shelf algorithms relying only on rational arithmetic. Section 3 describes the bisectors and (pre)geodesics for the five models, and discusses on degenerate cases for which the dual Delaunay complex is not a triangulation. In §4, we present a connection between the spaces of symmetric positive-definite 2×2 matrices of constant determinant and hyperbolic geometry. Finally, section 5 concludes this work. Appendix A reformulates our former work [25] in arbitrary dimension for sake of completeness.

1.1 Prior work

Since we consider the general d -dimensional setting, let us recall only prior work tackling the hyperbolic Voronoi diagram constructions in *arbitrary dimension*. Boissonnat and Yvinec [12] (pp. 449-454) proved that the complexity of the hyperbolic Voronoi diagram of a n -point set $\mathcal{P} \in \mathbb{H}^d(-1)$ is $\Theta(n^{\lceil \frac{d}{2} \rceil})$ using the Poincaré d -dimensional upper half-space model (U). They proceed by exhibiting an injective correspondence between the Euclidean and the hyperbolic diagrams using two successive projections. Nielsen and Nock [25] showed that the hyperbolic Voronoi diagram in the Klein ball model (K) amounts to compute a clipped power diagram [1]. Appendix A recalls this construction, extending [25] to arbitrary dimension. Bogdanov et al. [5] proved that the hyperbolic Delaunay triangulation (dual graph⁴ of the hyperbolic Voronoi diagram) in the Poincaré ball model (P) can be obtained by removing the simplices of the Euclidean Delaunay triangulation intersecting the bounding sphere [31]. Their approach requires only rational arithmetic.⁵

³For spherical geometry, the Gaussian curvature of the d -dimensional sphere of radius r is $\kappa = \frac{1}{r^2}$. The curvature tends to 0 (flat) when $r \rightarrow \infty$.

⁴The Delaunay complex is however not always a triangulation when points are in degenerate positions. See Section 3.

⁵However, we need to stick to the Poincaré model since conversion formula may introduce square root operations.

In this paper, we study the hyperbolic Voronoi diagram using the lesser known Beltrami hemisphere model [14] (B) and hyperboloid model (L), and show that the hyperbolic Voronoi diagram in those models amount to compute an affine diagram.

1.2 Applications

Hyperbolic Voronoi diagrams find applications in various fields of computer science. In computer graphics, Walter [28] proposed an hyperbolic image browser with its user-friendly interactive interface. In network, Tanuma et al. [27] extended the greedy geometric routing of Kleinberg [22] using the dual structure of hyperbolic Voronoi diagrams. In information geometry [20], the Riemannian geometry induced by the Fisher information matrix of location-scale families of probability distributions (e.g., normal, Cauchy or Laplace distributions) amounts to hyperbolic geometry $\mathbb{H}^d(\kappa)$, where the curvature constant κ depends on the standard density of the location-scale family. It follows that the statistical Voronoi diagrams with respect to the Fisher-Rao Riemannian distance [20] amounts to compute hyperbolic Voronoi diagrams. Hyperbolic geometry has been used in machine learning for embedding hierarchical structures with low distortions (e.g., [21]).

2 Hyperbolic Voronoi diagram in the Beltrami hemisphere model

The d -dimensional hyperbolic space can be studied using various analytic models embedded in \mathbb{R}^{d+1} using an extra dimension [14] denoted by x_0 . The hemisphere model $\mathcal{S}^+ \subset \mathbb{R}^{d+1}$ of hyperbolic space with constant curvature $\kappa = -\frac{1}{r^2}$ is defined on the positive half-sphere of radius $r = \sqrt{-\frac{1}{\kappa}}$:

$$\mathcal{S}^+ = \left\{ x \in \mathbb{R}^{d+1} \left| \sum_{i=0}^d x_i^2 = r^2 = -\frac{1}{\kappa} \text{ and } x_0 > 0 \right. \right\}. \quad (2)$$

Although less prominent in the literature, this hemisphere model was first reported by Beltrami [3] in 1868. The hyperbolic distance between two points p and p' on \mathcal{S}^+ is expressed [23] in the hemisphere model by:

$$d_B(p, p') = \operatorname{arccosh} \left(1 + \frac{1 - \langle p, p' \rangle_E}{\langle p, a \rangle_E \langle p', a \rangle_E} \right), \quad (3)$$

where point a denotes the southern pole of the sphere of radius $r = \sqrt{-\frac{1}{\kappa}}$: $a = (-r, 0, \dots, 0)$, $\operatorname{arccosh}(x) = \log(x + \sqrt{x^2 - 1})$ for $x \geq 1$, and $\langle p, p' \rangle_E = \sum_{i=0}^d p_i p'_i$ is the Euclidean inner product. We use the subscript E to distinguish this inner product from the Lorentzian inner product introduced in Section 3.

It follows from Eq. 3 that we have:

$$\cosh(d_B(p, p')) - 1 = \frac{1 - \langle p, p' \rangle}{r^2 p_0 p'_0}, \quad (4)$$

where $\cosh(x) = \frac{e^x + e^{-x}}{2}$ is the hyperbolic cosine function. Thus the bisector $\operatorname{Bi}_B(p, p')$ of two points p and p' on the hemisphere model is thus expressed by:

$$\text{Bi}_B(p, p') : \frac{1 - \langle p, x \rangle_{\mathbb{E}}}{r^2 p_0 x_0} = \frac{1 - \langle p', x \rangle_{\mathbb{E}}}{r^2 p'_0 x_0}, \quad (5)$$

$$\text{Bi}_B(p, p') : \sum_{i=1}^d x_i \left(\frac{p'_i}{p'_0} - \frac{p_i}{p_0} \right) + \frac{1}{p_0} - \frac{1}{p'_0} = 0, \quad x \in \mathcal{S}^+. \quad (6)$$

Observe that the bisector relaxed to \mathbb{R}^{d+1} is a hyperplane with the coefficient corresponding to the term x_0 vanishing (that is, a vertical hyperplane). Therefore the bisector on the hemisphere is a vertical $(d-1)$ -sphere.

To compute the hyperbolic Voronoi diagram on the Beltrami hemisphere, we can thus choose hyperplane $H_0 : x_0 = 0$, compute the affine diagram, and clip it with the ball $\sum_{i=1}^d x_i^2 < r^2$. We then either lift vertically this diagram onto the hemisphere, or manipulate the diagram internally using its affine representation on H_0 . (For example, point location can be handled directly on H_0 .)

On hyperplane H_0 , we write the bisector equation as:

$$\text{Bi}_B(p, p') : \left\langle x, \frac{p'}{p'_0} - \frac{p}{p_0} \right\rangle_{E^d} + \frac{1}{p_0} - \frac{1}{p'_0} = 0, \quad (7)$$

where $\langle \cdot, \cdot \rangle_{E^d}$ denotes the d -dimensional Euclidean dot product on coordinates x_1, \dots, x_d . Affine diagrams can be built equivalently using power diagrams [1]: A power diagram for a given a set $\mathcal{B} = \{B_1, \dots, B_n\}$ of n balls (with $B_i = \text{Ball}_E(c_i, w_i = r_i^2)$ for $i \in \{1, \dots, n\}$), is defined as the minimization diagram [11] of the corresponding n functions:

$$D_i(x) = \langle c_i - x, c_i - x \rangle_{\mathbb{E}} - w_i, \quad (8)$$

where w_i is the weight associated to center point c_i . The power bisector $B_{\Pi}(B_i, B_j)$ of any two distinct balls $B_i = \text{Ball}_E(c_i, w_i)$ and $B_j = \text{Ball}_E(c_j, w_j)$ is the *radical hyperplane* [1] of equation:

$$\text{Bi}_{\Pi}(B_i, B_j) : 2\langle x, c_j - c_i \rangle_{\mathbb{E}} + \langle c_i, c_i \rangle_{\mathbb{E}} - \langle c_j, c_j \rangle_{\mathbb{E}} + w_j - w_i = 0. \quad (9)$$

The last equation shows that power diagrams are additive weighted (ordinary) Voronoi diagrams [12].

To find the equivalence of the Beltrami hemisphere affine diagram with a power diagram, we map the points p to equivalent balls B with centers c and weights w such that:

$$c = \frac{p}{2p_0}, \quad w = \frac{1}{p_0} + \langle c, c \rangle_{\mathbb{E}} = \frac{1}{p_0} + \frac{\langle p, p \rangle_{\mathbb{E}}}{4p_0^2}.$$

This calculation requires only rational arithmetic but input shall be given using $d+1$ coordinates. (Klein hyperbolic Voronoi diagram used d -coordinates but requires algebraic coordinates, see Appendix A)

Although the worst-case combinatorial complexity $O(n^{\lceil \frac{d}{2} \rceil})$ was already obtained in the Klein ball model [25], the Poincaré ball model [5], and the Poincaré upper space model [12], this novel hemisphere construction allows us to use off-the-shelf power diagram constructions to build the hyperbolic Voronoi diagram using only rational arithmetic. Note that since the hyperbolic Voronoi diagram is a particular case of the Riemannian Voronoi diagram, it follows that the worst-case infinitesimally-scaled Euclidean Voronoi diagram (from equivalent polytopes on the $d+1$ -dimensional curve of moments [12]) can be obtained. Therefore the complexity of the hyperbolic Voronoi diagram is $\Theta(n^{\lceil \frac{d}{2} \rceil})$.

3 Voronoi bisectors and (pre)geodesics in the five standard models

Hyperbolic geometry can be studied under the framework of geodesic metric spaces [13]. A metric space (\mathbb{X}, d) is geodesic if and only if there exists a function γ such that for any pair of points $(p, q) \in \mathbb{X}^2$ and any pair of scalar $(s, t) \in [0, 1]^2$, we have:

$$d(\gamma(p, q; s), \gamma(p, q; t)) = |s - t| d(p, q),$$

with $\gamma(p, q; 0) = p$ and $\gamma(p, q; 1) = q$. Complete Riemannian manifolds are geodesic metric spaces. Riemannian geodesics are parameterized curves with constant speed (or equivalently are parameterized by arc length). Pregeodesics $\Gamma(p, q)$ are the traces of geodesics $\gamma(p, q; t)$:

$$\Gamma(p, q) := \{\gamma(p, q; t) : t \in [0, 1]\}.$$

Table 1 summarizes the Riemannian metrics and the Riemannian distances for the Beltrami hemisphere (B), the Poincaré upper half-space (U), the Poincaré ball (P), the Klein ball (K), and the Lorentz hyperboloid (L) models. The five model domains are $(r = \sqrt{-\frac{1}{\kappa}})$:

$$\mathcal{U}^+ = \{(x_0, r, x_2, \dots, x_d) \mid x_0 > 0\} \text{ (upper space),} \quad (10)$$

$$\mathcal{P} = \left\{ (0, x_1, \dots, x_d) \mid \sum_{i=1}^d x_i^2 < r^2 \right\} \text{ (Poincaré ball),} \quad (11)$$

$$\mathcal{S}^+ = \left\{ (x_0, x_1, \dots, x_d) \mid \sum_{i=0}^d x_i^2 < r^2 \text{ and } x_0 > 0 \right\} \text{ (Beltrami hemisphere),} \quad (12)$$

$$\mathcal{K} = \left\{ (r, x_1, \dots, x_d) \mid \sum_{i=1}^d x_i^2 < r^2 \right\} \text{ (Klein ball),} \quad (13)$$

$$\mathcal{L}^+ = \left\{ (x_0, x_1, \dots, x_d) \mid \sum_{i=1}^d x_i^2 - x_0^2 = -r^2 \text{ and } x_0 > 0 \right\} \text{ (Lorentz hyperboloid).} \quad (14)$$

The Poincaré and Klein ball models and the Poincaré upper half-space model have been often considered from an application point of view since their domain dimension does not need to increase the ambient dimension and they can be easily displayed on a computer screen.

These five models are all linked in \mathbb{R}^{d+1} as described in [14] (Figure 5, page 70). The maps from the hemisphere to the other models are either central or vertical projections explicited in [14]. Let us summarize the bisector expressions in those five standard models:

$$\text{Bi}_B(p, q) : \sum_{i=1}^d x_i \left(\frac{q_i}{q_0} - \frac{p_i}{p_0} \right) + \frac{1}{p_0} - \frac{1}{q_0} = 0, \quad (15)$$

$$\text{Bi}_K(p, q) : \left\langle x, q \sqrt{1 - \|p\|_E^2} - p \sqrt{1 - \|q\|_E^2} \right\rangle_E + \sqrt{1 - \|q\|_E^2} - \sqrt{1 - \|p\|_E^2} = 0, \quad (16)$$

$$\text{Bi}_P(p, q) : \langle x, x \rangle_E \left(\frac{1}{1 - \|p\|_E^2} - \frac{1}{1 - \|q\|_E^2} \right) + 2 \left\langle x, \frac{q}{1 - \|q\|_E^2} - \frac{p}{1 - \|p\|_E^2} \right\rangle_E +$$

Model	Riemannian metric ds^2	$\cosh \frac{d(p,q)}{\sqrt{-\kappa}}$, $d(\cdot, \cdot)$: Riemannian distance
Klein (K)	$-\kappa \left(\frac{ds_E^2}{1-\ x\ _E^2} + \frac{\langle x, dx \rangle_E}{(1-\ x\ _E^2)^2} \right)$	$\frac{1-\langle p, q \rangle_E}{\sqrt{(1-\ p\ _E^2)(1-\ q\ _E^2)}}$
Poincaré (P)	$-\kappa \frac{4ds_E^2}{(1-\ x\ _E^2)^2}$	$1 + \frac{2\ p-q\ _E^2}{(1-\ p\ _E^2)(1-\ q\ _E^2)}$
Upper (U)	$-\kappa \frac{ds_E^2}{x_d^2}$	$1 + \frac{\ p-q\ _E^2}{2p_d q_d}$
Hyperboloid (L)	$\kappa dx_0^2 + ds_E^2$	$\frac{\langle p, q \rangle_L}{\kappa}$
Hemisphere (B)	$\frac{\sum_{i=0}^d dx_i^2}{x_0^2}$	$1 + \frac{1-\langle p, q \rangle_E}{\kappa p_0 q_0}$

Table 1: Models of real hyperbolic geometry $\mathbb{H}^d(\kappa)$ of constant section negative curvature κ as Riemannian geometries: Riemannian metrics and distances. All models are conformal (angle-preserving) except Klein model that is not conformal (except at the origin).

$$\frac{\|p\|_E^2}{1-\|p\|_E^2} - \frac{\|q\|_E^2}{1-\|q\|_E^2} = 0, \quad (17)$$

$$\text{Bi}_L(p, q) : \langle x, q-p \rangle_L = (p_0 - q_0)x_0 + \sum_{i=1}^d (q_i - p_i)x_i = 0, \quad (18)$$

$$\text{Bi}_U(p, q) : \langle x, x \rangle_E \left(\frac{1}{p_d} - \frac{1}{q_d} \right) + 2 \left\langle x, \frac{q}{q_d} - \frac{p}{p_d} \right\rangle_E + \frac{\langle p, p \rangle_E}{p_d} - \frac{\langle q, q \rangle_E}{q_d} = 0. \quad (19)$$

$$(20)$$

where $\langle x, y \rangle_L = -x_0 y_0 + \sum_{i=1}^d x_i y_i$ denotes the Lorentzian⁶ inner product. Observe that the Lorentz bisectors relaxed to \mathbb{R}^{d+1} are hyperplanes all passing through the origin. (The pregeodesics are hyperbola arcs contained in a hyperplane passing through the origin.) The Lorentz hyperbolic Voronoi diagram can thus be obtained as the intersection of a $(d+1)$ -dimensional affine diagram with the hyperboloid upper sheet \mathbb{L}^+ . For odd dimension $d = 2k + 1$, we can thus build optimally the hyperbolic Voronoi diagram in the Lorentz model since $O(n^{\lceil \frac{d+1}{2} \rceil}) = O(n^{\lceil \frac{d}{2} \rceil}) = O(n^{k+1})$. That is, the extra dimension x_0 for odd parity does not exhibit the dimension gap in the combinatorial complexity of the Voronoi diagram. The hyperboloid model has been used by Galperin [18] to propose the *model centroid* in a closed-form expression. (Indeed the hyperbolic Kärcher centroid [19] does not admit an analytic expression.)

Table 2 characterizes the nature of the bisectors (bisecting sites) and pregeodesics (linking sites) for those models.

The pregeodesics $\Gamma_K(p, q)$ in the Klein model are line segments expressed as linear interpolations of the endpoints:

$$\Gamma_K(p, q) = \{(1-\beta)p + \beta q : \beta \in [0, 1]\}.$$

That is, the pregeodesics in the Klein model are obtained using the linear interpolation scheme $\text{LERP}(p, q; \beta) := (1-\beta)p + \beta q$. That is, we have: $\Gamma_K(p, q) = \{\text{LERP}(p, q, \beta) : \beta \in [0, 1]\}$.

Since the Klein model is a geodesic metric space (\mathcal{K}, d_K) , let us report the expression of Klein geodesics so that we have for any pair of points $(p, q) \in \mathcal{K}^2$ and any pair of scalar $(s, t) \in [0, 1]^2$:

$$d_K(\gamma_K(p, q; s), \gamma_K(p, q; t)) = |s - t| d_K(p, q),$$

⁶Although attributed to Hendrik Lorentz, the model is due to Karl Weierstrass [17].

Model	Pregeodesic	Bisector
Hemisphere	arc of circles	vertical spherical portion of the hemisphere
Klein ball	line segment	hyperplane
Poincaré ball	circular arc perpendicular to the bounding sphere, or straight lines passing through the origin	spherical portions, or hyperplanes passing through the origin when $\ p\ = \ q\ $
Upper half-space	arc of circles or vertical lines	spherical portions or hyperplanes
Hyperboloid	hyperbola	intersection of hyperplane passing through the origin with the hyperboloid

Table 2: Hyperbolic Voronoi diagrams: Characterization of pregeodesics and bisectors for the five standard models.

with $\gamma_K(p, q; 0) = p$ and $\gamma_K(p, q; 1) = q$.

Recall that the Klein metric distance $d_K(p, q)$ between any two points p and q in the unit disk centered at the origin with curvature $\kappa = -1$ is

$$d_K(p, q) = \operatorname{arccosh} \left(\frac{1 - p^\top q}{\sqrt{(1 - p^\top p)} \sqrt{(1 - q^\top q)}} \right).$$

We have $d_K(p, \gamma_K(p, q; \alpha)) = \alpha d_K(p, q)$ with $\gamma_K(p, q; \alpha) = (1 - c(\alpha))p + c(\alpha)q$. Thus we need to solve for $c(\alpha)$ in the equation:

$$\frac{a - bc(\alpha)}{\sqrt{a(a - 2bc(\alpha) + c'c(\alpha)^2)}} - d(\alpha) = 0,$$

with

$$\begin{aligned} a &:= 1 - p^\top p, \\ b &:= p^\top (q - p), \\ c' &:= (q - p)^\top (q - p), \\ d(\alpha) &:= \cosh(\alpha d_K(p, q)) \end{aligned}$$

Using symbolic calculations, we find the following solution:

$$c(\alpha) = \frac{ad(\alpha)\sqrt{(ac' + b^2)(d(\alpha)^2 - 1)} + ab(1 - d(\alpha)^2)}{ac'd(\alpha)^2 + b^2}. \quad (21)$$

Thus we get in closed-form the Klein geodesics $\gamma_K(p, q; \alpha)$ (albeit a large formula).

We check that our solution yields for all $(p, q) \in \mathcal{K}^2$ and $(s, t) \in [0, 1]^2$:

$$d_K(\gamma_K(p, q; s), \gamma_K(p, q; t)) = |s - t| d_K(p, q), \quad \forall s, t \in [0, 1].$$

We can use the Klein geodesics to efficiently compute the smallest enclosing ball of a finite point set \mathcal{P} in hyperbolic geometry [7]. With the expression of the Klein geodesic, we do not need to perform hyperbolic translations from and to the disk origin as in [8]. The algorithm for calculating an approximation of the smallest enclosing ball of $\mathcal{P} = \{p_1, \dots, p_n\}$ is:

Figure 1 depicts some degenerate cases in the ball models for co-spherical points centered at the origin, and their corresponding diagrams on the upper half-space model.

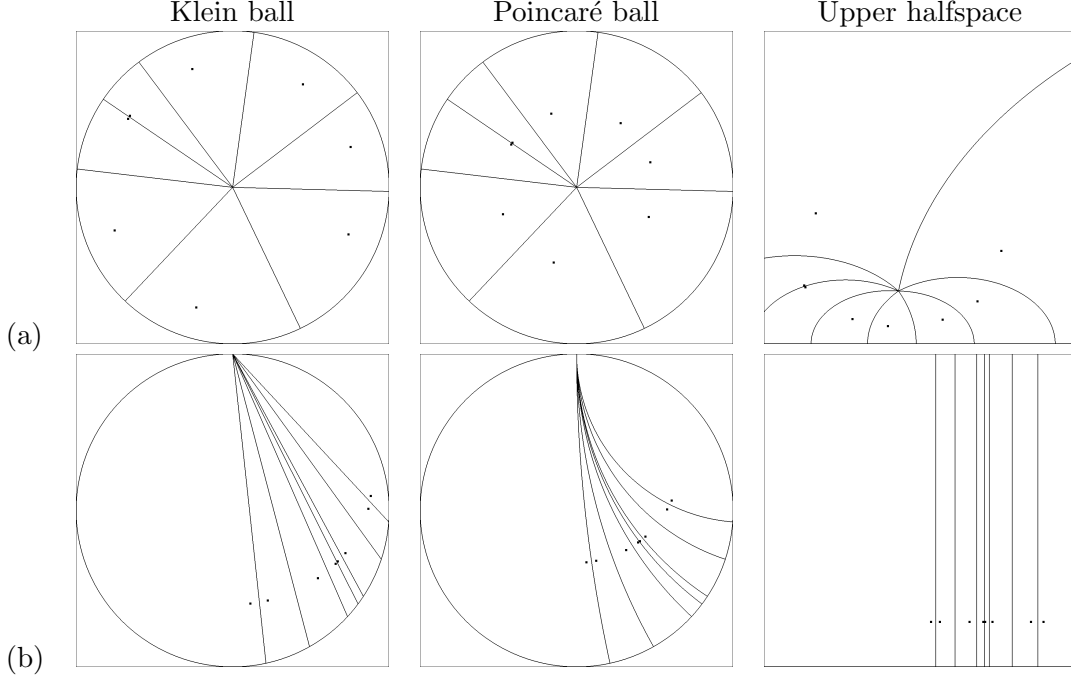


Figure 1: Degenerate hyperbolic Voronoi diagrams: (a): In the Poincaré/Klein ball models when point radii are all equal (wheel diagram with bisectors passing through the origin.) (b): In the upper halfspace when the d -th coordinate are all equal.

- Initialize $c_1 = p_1$
- Repeat t times: Let $c_{i+1} = \gamma_K \left(c_i, p_{f_i}, \frac{1}{i+1} \right)$ where p_{f_i} is the farthest point of \mathcal{P} to c_i . That is, we have $f_i = \arg \max_{j \in \{1, \dots, n\}} d_K(c_i, p_j)$.

The algorithm is proven to converge in [7] since the hyperbolic geometry is a Hadamard space.

It is well-known that for points in general position (no collinear nor co-spherical points), the dual of an ordinary Voronoi diagram is the unique Delaunay triangulation [12]. This duality holds for the hyperbolic Voronoi diagram and the hyperbolic Delaunay triangulation (with the empty sphere property), provided general position of the sites. Hyperbolic Voronoi diagrams can be fairly different from ordinary Voronoi diagram. For example, Figure 2 gives an example of the hyperbolic Voronoi diagram when all but one site are co-circular and close to the bounding circle with a single site centered at the ball center. In that case the dual Delaunay complex is not a triangulation although unique (a $(n - 1)$ -ary tree of depth 1). We refer to [9] for a stability analysis of the Delaunay triangulation on generic manifolds.

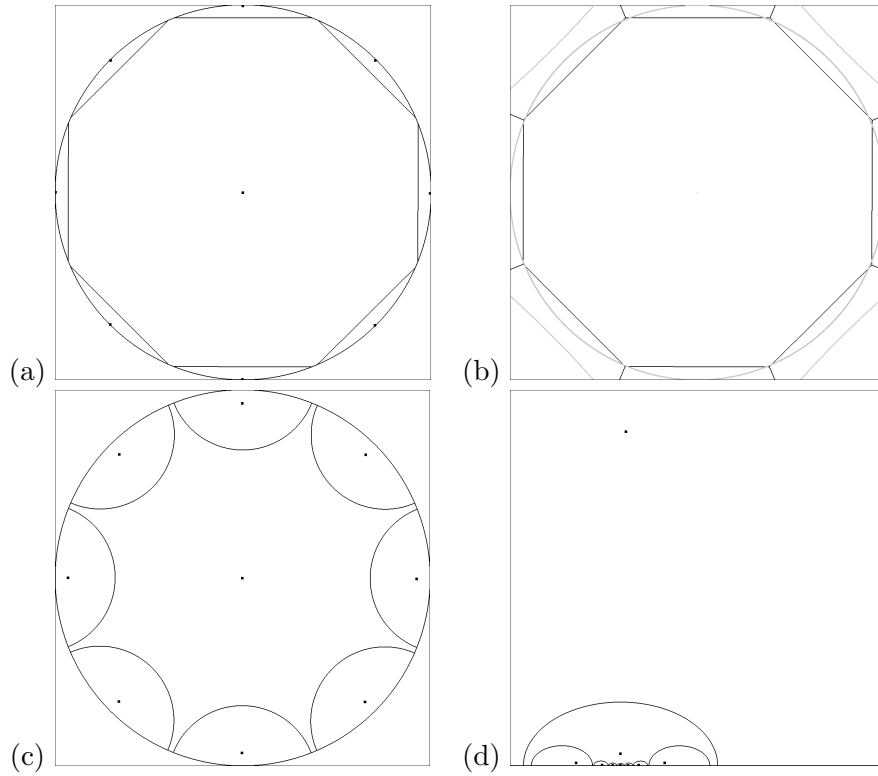


Figure 2: A hyperbolic Voronoi diagram with all cells unbounded ($n = 9$). The dual graph corresponds to a tree: (a) Klein, (b) equivalent power diagram, (c) Poincaré ball, and (d) Poincaré upper halfspace.

4 Hyperbolic geometry of the special symmetric positive-definite 2×2 matrices (SSPD)

Let $\text{SPD} = \{P \in \text{Mat}_{\mathbb{R}}(d, d) : P \succ 0\}$ denote the set of symmetric positive-definite (SPD) $d \times d$ matrices. Consider SPD as a Riemannian manifold [29] (M, g) equipped with the trace metric g defining at each tangent plane T_P the following inner product:

$$\forall A, B \in T_P, \quad g(A, B) = \langle A, B \rangle_P = \text{tr}(P^{-1}AP^{-1}B).$$

The SPD manifold is an open convex cone with geodesic equation $\ddot{P} - \dot{P}P^{-1}\dot{P} = 0$, and the geodesic $P_{12}(t)$ passing through P_1 and P_2 is parameterized as follows:

$$P_{12}(t) = P_1^{\frac{1}{2}} \exp(t \text{Log}(P_1^{-\frac{1}{2}} P_2 P_1^{-\frac{1}{2}})) P_1^{\frac{1}{2}},$$

where $\text{Log}(P)$ denotes the unique matrix logarithm of P since all eigenvalues of P are positive. The Riemannian induced distance is

$$\rho_{\text{SPD}}(P_1, P_2) = \sqrt{\sum_{i=1}^d \log^2 \lambda_i(P_1 P_2^{-1})},$$

where $\lambda_i(P) > 0$ denotes the i -th largest eigenvalue of matrix of $P \in \text{SPD}$. Observe that the Riemannian trace metric distance is scale-invariant:

$$\forall \lambda > 0, \quad \rho_{\text{SPD}}(\lambda P_1, \lambda P_2) = \rho_{\text{SPD}}(P_1, P_2).$$

When $d = 2$, we have

$$\text{SPD}_2 = \left\{ P = P(a, b, c) = \begin{bmatrix} a & c \\ c & b \end{bmatrix}, a > 0, ab - c^2 > 0 \right\},$$

and the largest eigenvalue λ_1 and smallest eigenvalue λ_2 can be calculated as follows:

$$\begin{aligned} \lambda_1(P) &= \frac{1}{2} \left(\text{tr}(P) + \sqrt{\text{tr}^2(P) - 4|P|} \right) \\ \lambda_2(P) &= \frac{1}{2} \left(\text{tr}(P) - \sqrt{\text{tr}^2(P) - 4|P|} \right), \end{aligned}$$

where $\text{tr}(P) = a + b$ denotes the matrix trace and $|P| = ab - c^2$ the matrix determinant.

The space SPD_2 can be foliated [30] (De Rham decomposition) as follows:

$$\text{SPD}_2 = \text{SSPD}_2(r) \times \mathbb{R}_{++},$$

where

$$\text{SSPD}_2(r) = \left\{ \begin{bmatrix} a & c \\ c & b \end{bmatrix}, a > 0, ab - c^2 = r \right\}.$$

The space $\text{SSPD}_2(r)$ denotes the space of special symmetric positive-definite matrices (SSPD) with prescribed determinant equal to r . For any $r > 0$, the $\text{SSPD}_2(r)$ is a totally geodesic submanifold of constant negative curvature $\kappa = -1/2$, and thus is isometric to the 2D hyperbolic geometry

with curvature $-1/2$. It follows that we have for matrices P_1 and P_2 in $\text{SSPD}(r)$ the following expression of the Riemannian matrix trace distance:

$$\rho_{\text{SSPD}_2}(P_1, P_2) = \rho_{\text{SSPD}_2} \left(\frac{P_1}{\sqrt{|P_1|}}, \frac{P_2}{\sqrt{|P_2|}} \right) = \sqrt{2} \rho_K \left(k \left(\frac{P_1}{\sqrt{|P_1|}} \right), k \left(\frac{P_2}{\sqrt{|P_2|}} \right) \right), \quad (22)$$

where ρ_K denotes the hyperbolic distance with curvature -1 expressed using the Klein unit disk model:

$$\rho_K(k_1, k_2) = \text{arccosh} \left(\frac{1 - k_1 \cdot k_2}{\sqrt{1 - k_1 \cdot k_1} \sqrt{1 - k_2 \cdot k_2}} \right),$$

where $p \cdot q = \langle p, q \rangle_E$ denotes the Euclidean inner product (dot product). The map $k : \text{SPD} \rightarrow \mathbb{R}^2$ transforms positive-definite matrices $P = P(a, b, c)$ to corresponding points on the Klein unit disk as follows:

$$k(P) = \left(\frac{a^2 + 2a - b^2 - 2b}{a^2 + 2a + b^2 + 2b + 2 + 2c^2}, \frac{2c(a + b + 2)}{a^2 + 2a + b^2 + 2b + 2 + 2c^2} \right). \quad (23)$$

Here, notice that we considered the Klein unit disk for the hyperbolic geometry model of curvature $\kappa < 0$, and we have:

$$\rho_{K, \kappa}(k_1, k_2) = \sqrt{-\frac{1}{\kappa}} \rho_K(k_1, k_2).$$

Thus, we have $\rho_{K, -\frac{1}{2}}(k_1, k_2) = \sqrt{2} \text{arccosh} \left(\frac{1 - k_1 \cdot k_2}{\sqrt{1 - k_1 \cdot k_1} \sqrt{1 - k_2 \cdot k_2}} \right)$.

Instead of using the Klein model, we can also use the Poincaré disk (P) model

$$\forall P_1, P_2 \in \text{SSPD}_2(r), \quad \rho_{\text{SSPD}_2}(P_1, P_2) = \sqrt{2} \rho_P \left(w \left(\frac{P_1}{\sqrt{|P_1|}} \right), w \left(\frac{P_2}{\sqrt{|P_2|}} \right) \right), \quad (24)$$

where

$$\rho_P(z_1, z_2) = 2 \text{arctanh} \left(\frac{|z_1 - z_2|}{|1 - \bar{z}_1 z_2|} \right),$$

$\text{arctanh}(x) = \frac{1}{2} \log \frac{1+x}{1-x}$, and $w : \text{SPD}_2 \rightarrow \mathbb{C}$ denotes the mapping:

$$w(P) = \frac{a - b}{2 + a + b} + i \frac{c}{2 + a + b}. \quad (25)$$

We can also use the hyperboloid model (L), and have

$$\forall P_1, P_2 \in \text{SSPD}_2(r), \quad \rho_{\text{SSPD}_2}(P_1, P_2) = \sqrt{2} \rho_L \left(h \left(\frac{P_1}{\sqrt{|P_1|}} \right), h \left(\frac{P_2}{\sqrt{|P_2|}} \right) \right), \quad (26)$$

where

$$\rho_L(h_1, h_2) = \text{arccosh}(-\langle h_1, h_2 \rangle_L),$$

with $\langle p, q \rangle_L = -p_1 q_1 + p_2 q_2 + p_3 q_3$, and $h : \text{SPD}_2 \rightarrow \mathbb{R}^3$ denotes the mapping of SPD matrices onto the upper sheet of the hyperboloid:

$$h(P) = \begin{bmatrix} \frac{a+b}{2} \\ \frac{a-b}{2} \\ c \end{bmatrix} \quad (27)$$

When $d > 2$, the space SPD_d can be foliated [30] as $\text{SPD}_d = \text{SSPD}_d \times \mathbb{R}_{++}$ (De Rham decomposition). SPD is interpreted as a foliated manifold with leaves $\text{SSPD}_d(r)$ of codimension 1, where $\text{SSPD}_d(r)$ denotes the space of special symmetric positive-definite $d \times d$ matrices with prescribed determinant equal to r . We can interpret SSPD_d as the following quotient space:

$$\text{SSPD}_d(1) \cong \text{SL}(d)/\text{SO}(d).$$

The spaces $\text{SSPD}_d(r)$ are Einstein submanifolds of SPD_d .

5 Conclusion

In the Klein ball model, we extended the planar case [25] and proved that the hyperbolic Voronoi diagram of a finite point set in arbitrary dimension is affine. It followed a simple method to optimally calculate the Klein hyperbolic Voronoi diagram by computing a corresponding power diagram clipped to the bounding sphere. This method however required non-rational arithmetic (square root operations in the denominator) on d -dimensional coordinates as noticed in [5]. To overcome this drawback, we described a novel approach in the hemisphere model, and showed that the hyperbolic Voronoi diagram also amounts to compute an affine diagram using only rational arithmetic on $(d + 1)$ -dimensional coordinates. From the view point of computational geometry, those various analytical models of hyperbolic space allow one to take advantage of the merits of each model. The Poincaré/Klein ball models are both conformal⁷ at the origin with geodesics passing through the origin being straight lines. For geodesic walking-type algorithms like computing the hyperbolic centroid, Barbaresco [2] considered the Poincaré ball model and perform a hyperbolic translation at each step to set the current point to the origin in order to ensure that geodesics departing from that current point are straight line segments. This could have been also performed using the Klein model. When manipulating these models, we may perform a hyperbolic rigid motion [23] to choose a convenient origin [4].⁸

Acknowledgments

Frank Nielsen would like to acknowledge email correspondence with Dr. Olivier Devillers on this topic [6] that considers the space of spheres [10] for tackling the hyperbolic Voronoi and hyperbolic Delaunay complex [31].

References

- [1] Franz Aurenhammer. Power diagrams: Properties, algorithms and applications. *SIAM Journal of Computing*, 16(1):78–96, 1987.
- [2] Frédéric Barbaresco. Interactions between symmetric cone and information geometries: Bruhat-Tits and Siegel spaces models for high resolution autoregressive Doppler imagery. In *Emerging Trends in Visual Computing (ETVC)*, volume LNCS 5416, pages 124–163, 2008.

⁷Preserving angles. That is, the metric is locally a scaled Euclidean metric (identity matrix).

⁸Orientation preserving isometries in 2D consists of all fractional linear transformations with real coefficients and unit determinant. That is the group of Möbius transformations ($\text{PSL}_2\mathbb{R}$). The real hyperbolic plane is then identified with the complex hyperbolic line. Orientation preserving isometries in 3D can be identified with $\text{PSL}_2\mathbb{C}$. That is, all fractional linear transformations of the plane of points at infinity with complex coefficients, see [24].

- [3] Eugenio Beltrami. Teoria fondamentale degli spazii di curvatura costante. *Annali di Matematica Pura ed Applicata (1867 - 1897)*, 2:232–255, 1868. in italian.
- [4] Marshall W. Bern and David Eppstein. Optimal Möbius transformations for information visualization and meshing. In *Workshop on Algorithms and Data Structures (WADS)*, pages 14–25, 2001.
- [5] Mikhail Bogdanov, Olivier Devillers, and Monique Teillaud. Hyperbolic Delaunay triangulations and Voronoi diagrams made practical. In *Spanish Meeting on Computational Geometry*, pages 113–116, 2011.
- [6] Mikhail Bogdanov, Olivier Devillers, and Monique Teillaud. Hyperbolic Delaunay complexes and Voronoi diagrams made practical. Rapport de recherche RR-8146, INRIA, November 2012.
- [7] Marc Arnaudon and Frank Nielsen. On approximating the Riemannian 1-center. *Computational Geometry*, volume 46, number 1, pages 93–104, 2013.
- [8] Frank Nielsen and Gaëtan Hadjeres. Approximating covering and minimum enclosing balls in hyperbolic geometry. In *International Conference on Geometric Science of Information (GSI)*, pages 586–594, 2015.
- [9] Jean-Daniel Boissonnat, Ramsay Dyer, and Arijit Ghosh. Stability of Delaunay-type structures for manifolds. In *Symposium on Computational Geometry*, pages 229–238, 2012.
- [10] Jean-Daniel Boissonnat, Frank Nielsen, and Richard Nock. Bregman Voronoi diagrams. *Discrete & Computational Geometry*, 44(2):281–307, 2010.
- [11] Jean-Daniel Boissonnat, Camille Wormser, and Mariette Yvinec. Curved Voronoi diagrams. In *Effective Computational Geometry for Curves and Surfaces*, Mathematics + Visualization, pages 67–116. Springer, 2007.
- [12] Jean-Daniel Boissonnat and Mariette Yvinec. *Algorithmic Geometry*. Cambridge University Press, New York, NY, USA, 1998.
- [13] Martin R. Bridson and Andre Haefliger. *Metric Spaces of Non-Positive Curvature*. Grundlehren Der Mathematischen Wissenschaften. Springer, 2009.
- [14] James W Cannon, William J Floyd, Richard Kenyon, and Walter R Parry. Hyperbolic geometry. In *Flavors of Geometry*, pages 59–115. Cambridge University Press, 1997.
- [15] Timothy M. Chan. Output-sensitive results on convex hulls, extreme points, and related problems. *Discrete & Computational Geometry*, 16(4):369–387, 1996.
- [16] Boris N. Delaunay. Sur la sphère vide. *Bulletin of Academy of Sciences of the USSR*, (6):793–800, 1934.
- [17] Florin Diacu. *Relative Equilibria of the Curved N-Body Problem*. Atlantis Series in Dynamical Systems. Atlantis Press, 2012.

- [18] G.A. Galperin. A concept of the mass center of a system of material points in the constant curvature spaces. *Communications in Mathematical Physics*, 154:63–84, 1993.
- [19] Hermann Karcher. Riemannian center of mass and mollifier smoothing. *Communications on Pure and Applied Mathematics*, 30(5):509–541, 1977.
- [20] Robert E. Kass and Paul W. Vos. *Geometrical foundations of asymptotic inference*. Wiley series in probability and statistics: Probability and statistics. Wiley, 1997.
- [21] Nickel, Maximillian, and Douwe Kiela. In *International Conference on Machine Learning (ICML)*, pages 3779–3788, 2018.
- [22] Robert Kleinberg. Geographic routing using hyperbolic space. In *IEEE International Conference on Computer Communications (INFOCOM)*, pages 1902–1909, 2007.
- [23] Hongbo Li, David Hestenes, and Alyn Rockwood. Geometric computing with clifford algebras. chapter A universal model for conformal geometries of Euclidean, spherical and double-hyperbolic spaces, pages 77–104. Springer-Verlag, London, UK, UK, 2001.
- [24] John Milnor. Hyperbolic geometry: The first 150 years. *Bull.AMS*, 6:9–24, 1982.
- [25] Frank Nielsen and Richard Nock. Hyperbolic Voronoi diagrams made easy. In *International Conference on Computational Science and Its Applications (ICCSA)*, pages 74 –80, march 2010.
- [26] Atsuyuki Okabe, Barry Boots, and Kokichi Sugihara. *Spatial tessellations: concepts and applications of Voronoi diagrams*. John Wiley & Sons, Inc., New York, NY, USA, 1992.
- [27] Toshihiro Tanuma, Hiroshi Imai, and Sonoko Moriyama. Revisiting hyperbolic Voronoi diagrams in two and higher dimensions from theoretical, applied and generalized viewpoints. In Marina Gavrilova, C. Tan, and Mir Mostafavi, editors, *Transactions on Computational Science XIV*, volume 6970 of *Lecture Notes in Computer Science*, pages 1–30. Springer Berlin / Heidelberg, 2011.
- [28] Jörg A. Walter. H-MDS: A new approach for interactive visualization with multidimensional scaling in the hyperbolic space. *Information Systems*, 29(4):273–292, 2004.
- [29] Moakher, Maher, and Mourad Zřai. The Riemannian geometry of the space of positive-definite matrices and its application to the regularization of positive-definite matrix-valued data *Journal of Mathematical Imaging and Vision*, 40(2):171-187, 2011.
- [30] Maass, Hans. Siegel’s modular forms and Dirichlet series: course given at the University of Maryland, 1969-1970 *Springer*, Vol. 216, 2006.
- [31] Frank Nielsen. On Voronoi diagrams on the information-geometric Cauchy manifolds *Entropy*, 22(7):713, 2020.

A Hyperbolic Voronoi diagrams in the Klein projective ball model

This appendix extends [25] to arbitrary dimension. In the Klein ball model $\mathcal{K}(\kappa)$, the hyperbolic geometry of curvature $\kappa = -\frac{1}{r^2}$ is embedded [13] inside a Euclidean ball $\mathbb{B} = \{x \in \mathbb{R}^d \mid \|x\|_E < r\}$ of radius r with the corresponding Klein hyperbolic distance $d_K(p, q)$ between two points p and q expressed by:

$$d_K(p, q) = \sqrt{-\kappa} \times \operatorname{arccosh} \left(\frac{1 - \langle p, q \rangle_E}{\sqrt{(1 - \|p\|_E^2)(1 - \|q\|_E^2)}} \right), \quad (28)$$

where $\operatorname{arccosh}(x) = \log(x + \sqrt{x^2 - 1})$ for $x \geq 1$.

Consider the Klein bisector $\operatorname{Bi}_K(p, q)$ of any two distinct points p and q :

$$\operatorname{Bi}_K(p, q) = \{x \in \mathcal{K}(\kappa) \mid d_K(p, x) = d_K(q, x)\}, \quad (29)$$

Since $\operatorname{arccosh}(x)$ is a monotonic function preserving the distance order and $\sqrt{-\kappa}$ is a multiplicative constant, it follows that:

$$\operatorname{Bi}_K(p, q) = \left\{ x \in \mathbb{B}^d \mid \frac{1 - \langle p, x \rangle_E}{\sqrt{(1 - \|p\|_E^2)(1 - \|x\|_E^2)}} = \frac{1 - \langle q, x \rangle_E}{\sqrt{(1 - \|q\|_E^2)(1 - \|x\|_E^2)}} \right\}. \quad (30)$$

Therefore, the bisector $B_K(p, q)$ is the loci of the points x satisfying:

$$\left\langle x, q\sqrt{1 - \|p\|_E^2} - p\sqrt{1 - \|q\|_E^2} \right\rangle_E + \sqrt{1 - \|q\|_E^2} - \sqrt{1 - \|p\|_E^2} = 0. \quad (31)$$

This is a linear equation $\langle a, x \rangle_E + b = 0$ in x , with:

$$a = q\sqrt{1 - \|p\|_E^2} - p\sqrt{1 - \|q\|_E^2}, \quad b = \sqrt{1 - \|q\|_E^2} - \sqrt{1 - \|p\|_E^2}. \quad (32)$$

That is, Klein bisectors are hyperplanes. It follows that the Klein hyperbolic Voronoi diagram is an *affine diagram* [11] with all its Voronoi cells convex.⁹ Affine diagrams can be *universally* built from an equivalent power diagram [11]. The power distance $d_\Pi(B, x)$ of a point x to a Euclidean ball $B = \operatorname{Ball}_E(c, r)$ of center c and radius r is defined as:

$$d_\Pi(B, x) = \langle c - x, c - x \rangle_E - r^2. \quad (33)$$

Given a set $\mathcal{B} = \{B_1, \dots, B_n\}$ of n balls with $B_i = \operatorname{Ball}_E(c_i, r_i)$, the power diagram is defined as the minimization diagram [11] of the corresponding n functions:

$$D_i(x) = \langle c_i - x, c_i - x \rangle_E - r_i^2. \quad (34)$$

The power bisector $B_\Pi(B_i, B_j)$ of any two distinct balls $B_i = \operatorname{Ball}_E(c_i, r_i)$ and $B_j = \operatorname{Ball}_E(c_j, r_j)$ is the *radical hyperplane* [1] of equation:

$$B_\Pi(B_i, B_j) : 2\langle x, c_j - c_i \rangle_E + \langle c_i, c_i \rangle_E - \langle c_j, c_j \rangle_E + r_j^2 - r_i^2 = 0. \quad (35)$$

⁹It is a particular affine diagram since all its cells are guaranteed non-empty.

This power bisector linear equation shows that power diagrams are also affine diagrams. Let us report the mapping that associates to points in the Klein ball corresponding Euclidean balls so that their bisectors coincide pairwise. By identifying the bisector equation Eq. 31 with that of Eq. 9, we find that point p_i is mapped to a ball B_i of center c_i with squared radius r_i^2 , where:

$$c_i = c(B_i) = \frac{p_i}{2\sqrt{1 - \|p_i\|_E^2}}, \quad r_i^2 = r^2(B_i) = \frac{\|p_i\|_E^2}{4(1 - \|p_i\|_E^2)} - \frac{1}{\sqrt{1 - \|p_i\|_E^2}}. \quad (36)$$

Observe that the ball centers may span the full d -dimensional Euclidean space \mathbb{R}^d . The radii may be negative and are interpreted as balls with imaginary radii (or as weighted points with real weights, see Eq. 33). Solving for the quadratic expression¹⁰ of Eq. 36, we find that $r^2(p_i) < 0$ if and only if:

$$\|p_i\|_E^2 < 4(\sqrt{5} - 2) \simeq 0.944272. \quad (37)$$

Thus to compute the Klein hyperbolic Voronoi diagram of point set $\mathcal{P} = \{p_1, \dots, p_n\}$, we first construct a set of corresponding balls

$$\mathcal{B} = \{B_1 = \text{Ball}_E(c(p_1), r(p_1)), \dots, B_n = \text{Ball}_E(c(p_n), r(p_n))\}, \quad (38)$$

compute the power diagram¹¹ of \mathcal{B} , and consider the restriction of this diagram to the unit ball \mathbb{B}^d . Figure 3(a) and Figure 3(b) depict the Klein Voronoi diagram and corresponding power diagram, respectively. It follows another proof of the combinatorial complexity of the hyperbolic Voronoi diagram using the Klein model instead of the Poincaré upper halfspace [12] (pp. 449-454) or the Poincaré ball model [5]:

Theorem 1 *The hyperbolic Voronoi diagram of n d -dimensional points can be obtained in the Klein ball model as an equivalent power diagram clipped with the interior of the unit ball. The diagram has combinatorial complexity $O(n^{\lceil \frac{d}{2} \rceil})$ and can be built in optimal $O(n \log n + n^{\lceil \frac{d}{2} \rceil})$ time.*

Figure 3(a) displays the Klein hyperbolic Voronoi diagram built from an equivalent power diagram (Figure 3(b)). Note that all bounded Voronoi cells necessarily fall inside the ball, and therefore the construction can be made output-sensitive using Chan’s algorithm [15].

The following section describes the mapping functions to convert from the Klein model et the Poincaré ball, upper halfspace and Lorentz models.

B Converting Klein model to other models

We report formula¹² and their inverse for converting from/to Klein coordinates into the Poincaré ball (P), upper halfspace (U) and Lorentz coordinates(L):

¹⁰Let $l = \|p\|_E^2 \in [0, 1]$. We seek when $\frac{l}{4(1-l)} - \frac{1}{\sqrt{1-l}} < 0$. That is, we solve for the root of equation $l - 4\sqrt{1-l}$ in $[0, 1]$. This is a quadratic expression $l^2 + 16l - 16 = 0$ which admits a unique root in $[0, 1]$: $4(\sqrt{5} - 2)$.

¹¹Power diagrams can be computed in arbitrary dimension as convex hulls or halfspace intersections (unbounded polytope) using free software like QHull (<http://qhull.org>), CGAL (<http://www.cgal.org>) or LEDA (<http://www.algorithmic-solutions.com/leda/>).

¹²Wlog., we assume $\kappa = -1$. Otherwise, we first rescale by $\sqrt{-\frac{1}{\kappa}}$.

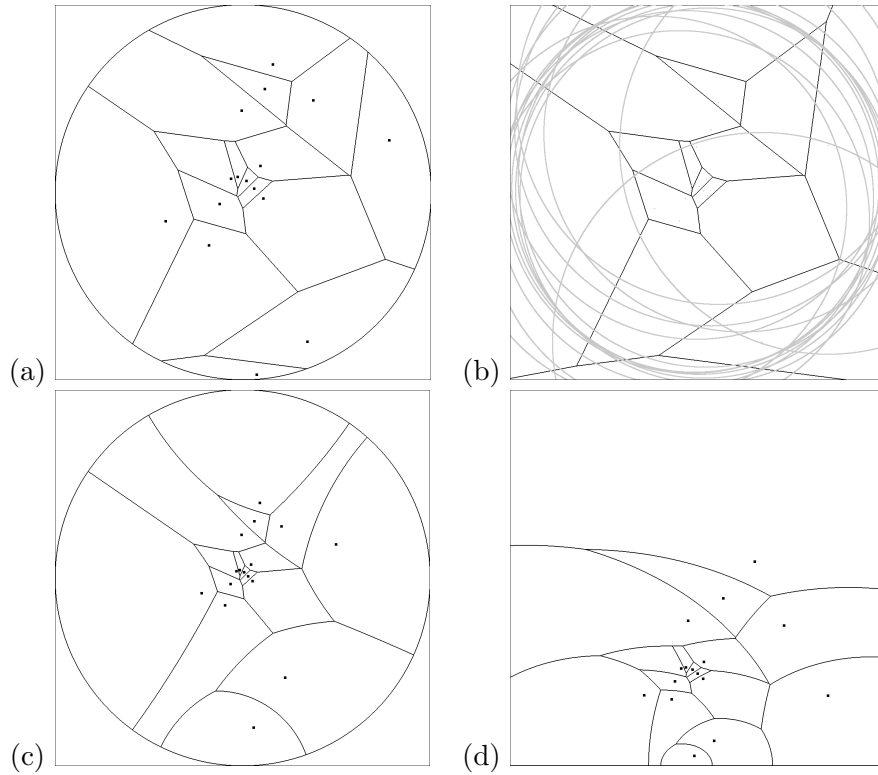


Figure 3: (a) The Klein Voronoi diagram calculated from the restriction of the power diagram (b) to the unit ball. Converting the Klein diagram into the Poincaré Voronoi diagram (c) and the upper half-space Voronoi diagram. Observe that the combinatorial complexity of the cells does not change ($n = 16$ points). The power diagram may have cells empty of sites and ball centers may be located outside the square of side length $r = \sqrt{-\frac{1}{\kappa}}$.

$$P_K(x) = \frac{x}{1 + \sqrt{1 - \|x\|_E^2}}, \quad (39)$$

$$K_P(x) = \frac{2x}{1 + \|x\|_E^2}, \quad (40)$$

$$U_K(x) = \frac{\left(1 - \frac{\|x\|_E^2}{1 + \sqrt{1 - \|x\|_E^2}}, x_1, \dots, x_{d-1}\right)}{1 - x_d}, \quad (41)$$

$$K_U(x) = \frac{(\|x\|_E^2 - 1, 2x_1, \dots, 2x_{d-1})}{1 + \|x\|_E^2}, \quad (42)$$

$$L_K(x) = \frac{(1, x_1, \dots, x_d)}{\sqrt{1 - \|x\|_E^2}}, \quad (43)$$

$$K_L(x) = \left(\frac{x_1}{x_0}, \dots, \frac{x_d}{x_0}\right). \quad (44)$$